



Single-particle reconstruction in cryo-EM based on three-dimensional weighted nuclear norm minimization

Chaoyan Huang^a, Tingting Wu^b, Juncheng Li^c, Bin Dong^d, Tieyong Zeng^{a,*}

^a Department of Mathematics, The Chinese University of Hong Kong, Shatin, NT, Hong Kong

^b School of Science, Nanjing University of Posts and Telecommunications, Nanjing, China

^c School of Communication & Information Engineering, Shanghai University, Shanghai, China

^d Beijing International Center for Mathematical Research (BICMR), Center for Machine Learning Research (CMLR), Peking University, China



ARTICLE INFO

Article history:

Received 4 August 2022

Revised 18 May 2023

Accepted 29 May 2023

Available online 5 June 2023

Keywords:

Single-particle reconstruction

Cryogenic electron microscopy

Forward-backward splitting algorithm

Three-dimensional weighted nuclear norm minimization

ABSTRACT

Single-particle reconstruction (SPR) in cryogenic electron microscopy (cryo-EM) aims at aligning and averaging two-dimensional micrographs to reconstruct a three-dimensional particle.

How to reconstruct micrographs from heavy noise is a crucial point for achieving better micrograph quality, and thus many methods focus on noise removal. However, new problems such as over-smoothing often occur in their results due to failure in handling heavy noise well. This paper proposes a three-dimensional weighted nuclear norm minimization (3DWNNM) model for SPR in the cryo-EM task to address these issues. Specifically, we design a minimization solver based on the forward-backward splitting algorithm to tackle our model efficiently. Under certain conditions, this solution has an energy-decaying feature and performs exceptionally well in reconstruction. Numerical experiments fully demonstrate the effectiveness and the robustness of the proposed method.

© 2023 Elsevier Ltd. All rights reserved.

1. Introduction

In 2017, Jacques Dubochet, Joachim Frank, and Richard Henderson were awarded the Nobel Prize in Chemistry for developing cryogenic electron microscopy (cryo-EM). A giant technological leap in cryo-EM has ensured the realization of near-atomic-resolution structures of biological macromolecules. As an essential structural biology research tool, cryo-EM is becoming increasingly prominent in structural biology. Together with X-ray crystallography and nuclear magnetic resonance (NMR), it is the cornerstone of high-resolution structural biology research. Recently, the research on single-particle reconstruction (SPR) in cryo-EM has attracted considerable attention. SPR in cryo-EM is a new technique to determine the three-dimensional (3D) structure of macromolecules, which uses the resulting set of noisy two-dimensional projection images taken in unknown directions to reconstruct the 3D structure of the molecule [1].

As a challenging and gratifying task, various techniques have been proposed for SPR, among which variational-based models are extensively utilized and have had remarkable success [2]. Generally, total variation (TV)-based models [3] and low rank-based

models [4] are two types of variational-based models that are commonly used. The reconstruction of TV-based models is mainly relied on gradient information, making the edge information well-preserved [5]. On the other hand, since the high-dimensional data inherently has a low-rank structure [6,7], the purpose of low rank-based models [8,9] is to recover the underlying low-rank matrix from its corrupted observation precisely and effectively. The nuclear norm regularizer, for example, is the tightest convex relaxation of the NP-hard rank minimization function [10]. However, several studies [11,12] have found that the nuclear norm-based low-rank methods generate sub-optimal results of the original rank minimization. The reason is that each singular value is considered identically, even though the large singular values which may contain more information. To better approximate the rank function, many nonconvex surrogates have been proposed, such as the Laplacian regularization [13], weighted nuclear norm [14], Schatten norm [15], and log-determinant function [16], and have shown promising results in various image processing tasks. Among them, the most popular one is the weighted nuclear norm minimization (WNNM) regularizer, which assigns varying weights to distinct unique values based on their physical relevance [17]. Continuing in this vein, Lv and Li [18] proposed an iterative decoupled method, which combined the fast transforms and the WNNM for image restoration. In [19], the authors proposed an effective WNNM-based nonconvex model for phase retrieval. The authors in

* Corresponding author.

E-mail address: zeng@math.cuhk.edu.hk (T. Zeng).

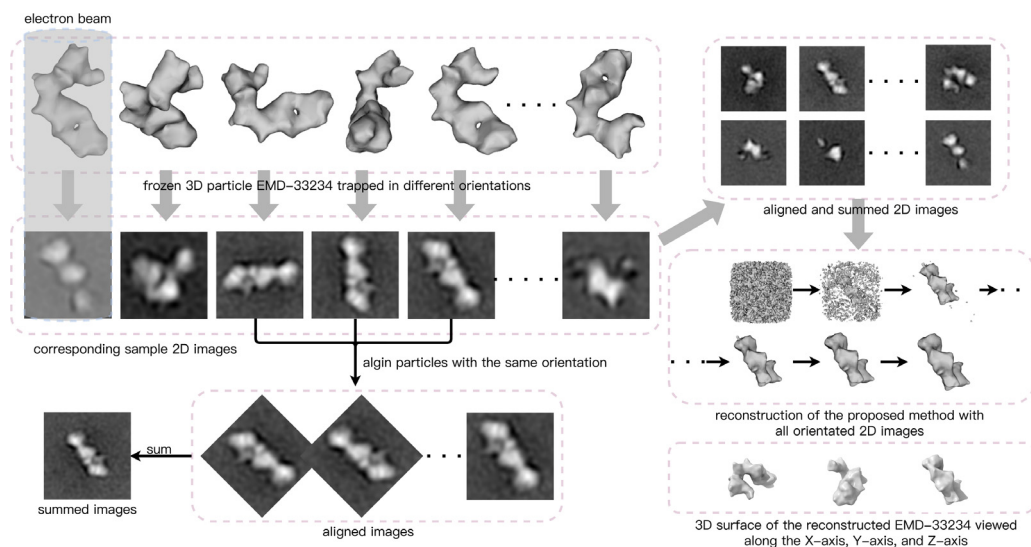


Fig. 1. The schematic diagram of single-particle reconstruction. Here are particles trapped in different orientations. When we shoot the particles with an electron beam, the orientation of the particles leaves a unique “shadow”, which contains all the 3-dimensional information of the particle compressed into a 2D image. Some particles are trapped in the same orientation, and so are their sampled 2D images. We select these images and rotate them in the same direction, and the aligned images are then added together. This summed image provides a more detailed view of the particle in this orientation. We perform this same process for the different orientations of the particle. As a result, the reconstruction of the proposed method with orientated 2D images

Jiang et al. [20] proposed a tubal nuclear norm-based model with tensors for imaging data recovery. All methods mentioned above demonstrate the robustness of the WNNM-based scheme. Inspired by this, in this paper, we aim to extend the WNNM-based model to three-dimension to handle the SPR task in cryo-EM.

As for the SPR in cryo-EM, there are not many methods currently available since cryo-EM imaging is still in an early stage, and it is a complicated and challenging task that many problems remain to be resolved [21]. In general, the signal-to-noise ratio (SNR) of cryo-EM data is very low. On the one hand, due to the lack of contrast enhancers in the solution, the micrographs acquired for cryo-EM exhibit low contrast. On the other hand, electron doses must be maintained low to protect biomolecules from radiation. Therefore, it is complicated to estimate the three-dimensional structure of molecules at such low SNR [22,23]. In fact, the process of estimating the three-dimension structure of a molecule involves averaging the two-dimension images to mitigate the effects of motion caused by the electron beam, thereby improving the SNR [24]. In general, the centroid of the particle needs to be identified first. However, due to the Fourier transform of the point spread function (PSF) in the microscope, estimating accurate characteristics of the contrast transfer function (CTF) is quite difficult [25]. Fortunately, according to the Fourier slice theorem, acquiring tomographic projections from known viewing directions is equivalent to sampling the three-dimension Fourier space. Therefore, the advantage of the Fourier space is that there is no need to rotate the numerator, i.e., projections can be computed quickly using off-the-shelf non-uniform fast Fourier transform (FFT) packages. In this case, the CTF is just a diagonal operator. Once the viewing directions of all experimental images are specified, the three-dimensional structure can be constructed using standard linear inversion techniques [26]. Following this, in this paper, we consider the reconstruction task with the known and fixed viewing directions. The schematic diagram of single-particle reconstruction is given in Fig. 1.

In this work, the orientations and positions are assumed to be known and fixed. Furthermore, based on this setting, Wang et al. [27] proposed a Fourier-based iterative method for cryo-EM particle reconstruction with the known orientations and positions prior. Later, considering the corruption of noise, Pan et al. [21] proposed a total variation regularization-based model

for SPR in cryo-EM. However, total variation regularization-based methods are susceptible to noise, and they will misinterpret noise as a boundary, resulting in a staircase effect or oversmoothing. As mentioned before, WNNM-based models are more robust than total variation-based models in many applications. Therefore, in this paper, we consider exploring a three-dimensional weighted nuclear norm minimization (3DWNNM) model to better suppress heavy noise in SPR tasks. In addition to the proposed reconstruction model, the minimization algorithm of the energy function is also crucial for SPR in cryo-EM. The classical algorithm includes the alternating minimization algorithm (AMA), the alternating direction method of multipliers (ADMM), and the forward-backward splitting (FBS), etc. Among them, the AMA was proposed to handle the convex problem, which separated the minimization function into two-block, and at least one of the blocks is assumed to be strongly convex [28]. The ADMM is frequently utilized in a variety of fields, and its convergence has been proved by updating two blocks of variables alternately [29]. However, Chen et al. [30] have proved that the direct extension of ADMM for multi-block convex minimization problems is not necessarily convergent. Different from ADMM, FBS can handle a more generic problem of minimizing the sum of two convex functions [31]. Specifically, the FBS consists of a forward gradient step on the differentiable part of the objective function, followed by a backward step on the other part. The FBS algorithm can generate a sparse solution with minimum processing cost. On the other hand, the FBS allows the method to build on existing analyses with the formal convergence of many existing gradient-based convex optimization algorithms. Given the advantageous qualities of the FBS algorithm, in this paper, we aim to adopt the FBS algorithm to solve the proposed model and analyze the convergence of our reconstruction model.

How to reconstruct micrographs from heavy noise is critical for improving micrograph quality. Many approaches focus on noise reduction. However, additional issues such as over-smoothing frequently appear in their results as a consequence of their inability to handle heavy noise adequately. To overcome this challenge, we propose a novel single-particle reconstruction model for three-dimensional cryogenic electron microscopy. The main contributions are as follows. Firstly, to overcome the over-smooth and the staircase effects of the TV-based reconstruction models,

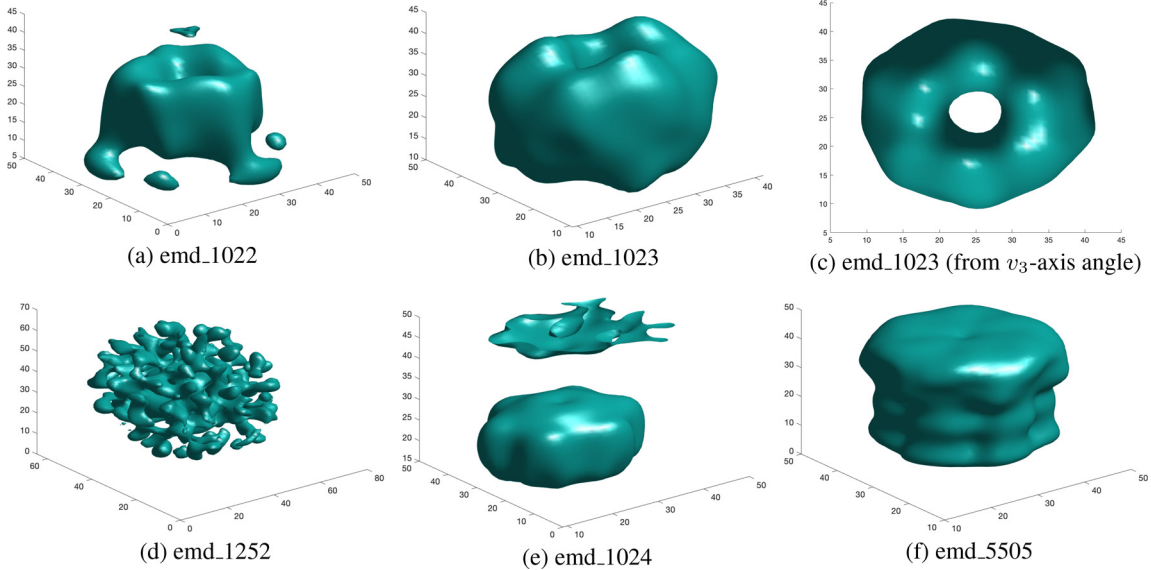


Fig. 2. Some examples of single-particles, including 'emd_1022', 'emd_1023', 'emd_1252', 'emd_1024', and 'emd_5505'.

we apply the low rank-based model to better suppress the noise in the SPR task. Secondly, treating different features the same is not conducive to the use of features, resulting in unsatisfactory reconstruction results. We use the weighted nuclear norm to assign different weights to different features so that the model can make better use of features and reconstruct results with better structure and details. Thirdly, as the SPR task has a three-dimensional structure, we extend the WNNM model to three-dimension and give the theoretical analysis of the three-dimensional weighted nuclear norm minimization (3DWNNM). Fourthly, we design an efficient and theoretically guaranteed algorithm for the proposed model, which can solve the model accurately. Experiments on SPR in cryo-EM show that the proposed method can provide more outstanding reconstruction results than several state-of-the-art methods.

The rest of this paper is organized as follows. In [Section 2](#), we first review the mathematical part of the cryo-EM reconstruction task, then the essential works of the WNNM method and the FBS algorithm are given. In [Section 3](#), we present the proposed 3DWNNM model and design the FBS-based algorithm for solving the developed model with the convergence analysis. In [Section 4](#), we provide the numerical results to demonstrate the superior performance of the proposed scheme. Finally, a conclusion is drawn in [Section 5](#).

2. Related works

2.1. The cryo-EM reconstruction task

Assume $\nu \in \mathbb{R}^{N \times N \times M}$ is a three-dimensional particle to be estimated, the rotation and the position of the particle are known and fixed, i.e., each image g_1, g_2, \dots, g_M is formed by rotating ν with three-dimensional rotation R_ω . Then we have the following formation

$$g_i = h_i \otimes S_{k_i} \int_{-\infty}^{\infty} R_{\omega_i}^* \nu \, d\nu_3 + b, \quad i = 1, \dots, M, \quad (1)$$

where h is the PSF, S_k is the 2D shift, \otimes is the convolution operation, R_ω^* is the adjoint operator of R_ω , and b is the noise, $\nu = (\nu_1, \nu_2, \nu_3)$ denotes the particle ν in the $\nu_1 \nu_2 \nu_3$ -coordinate system. When the angle ω_i of rotation R_{ω_i} changes, we can get M different slices $g_i, i = 1, 2, \dots, M$. To better understand, model (1) can be

condensed as

$$g_i = h_i \otimes S_{k_i} T \nu_i + b, \quad i = 1, \dots, M, \quad (2)$$

where T can be seen as a tomographic projection and $\nu_i \in \mathbb{R}^{N \times N}$, $i = 1, \dots, M$, represents M different slices [32,33]. After that, with the Fourier slice theorem, using project volume g_i to obtain M truncated Fourier slices corresponding to the particle ν in Cartesian coordinates $\omega_{k_1, k_2} = (\omega_{k_1}, \omega_{k_2}) = 2\pi(k_1, k_2)/N, k_1, k_2 \in \mathbb{Z}$, (k_1, k_2) is inside a ball in the Fourier domain as $\|(k_1, k_2)\| \leq \frac{N}{2}$. Suppose A is some projection, model (2) can be reformulated as

$$g = A(\nu) + b. \quad (3)$$

With the property of A and $\langle A(\nu), p \rangle = \langle \nu, A^*(p) \rangle$, where $p = (p_{k_1, k_2, m})$ is arbitrary collection of M truncated slices, we have

$$A^*(p) = \sum_{m=1}^M \sum_{k_1, k_2} \exp(i \langle R_m^{-1}(\omega_{k_1}, \omega_{k_2}, 0), \nu \rangle) h_m(\|\omega_{k_1, k_2}\|) p_{k_1, k_2, m}. \quad (4)$$

Then the A^*A operator can be given as

$$A^*A(p) = \sum_l p_{k_1, k_2, l} \sum_{m=1}^M \sum_{k_1, k_2} \exp(i \langle R_m^{-1}(\omega_{k_1}, \omega_{k_2}, 0), \nu \rangle) h_m(\|\omega_{k_1, k_2}\|)^2. \quad (5)$$

Note that the Eqs. (4) and (5) are needed when solving the proposed optimization model in [Section 3](#).

Based on the above fact, the authors in Wang et al. [27] proposed a conjugate gradient method for SPR in cryo-EM as

$$\min_{\nu} \|g - A(\nu)\|^2. \quad (6)$$

Although a solution can be found from (6), noise still apparently remains in the reconstructed particles. Late, in Pan et al. [21], two efficient models with regularizers were proposed as

$$\min_{\nu} \alpha \|g - A(\nu)\|^2 + \|\nu\|^2, \quad (7)$$

where α is a positive parameter, and

$$\min_{\nu} \alpha \|g - A(\nu)\|^2 + \|\nabla \nu\|_1, \quad (8)$$

where $\|\nabla \nu\|_1$ is the total variation regularizer. The reconstruction results from (7) are unsatisfactory, then they make an adaptive parameter to improve the model (7). With the improvement of the

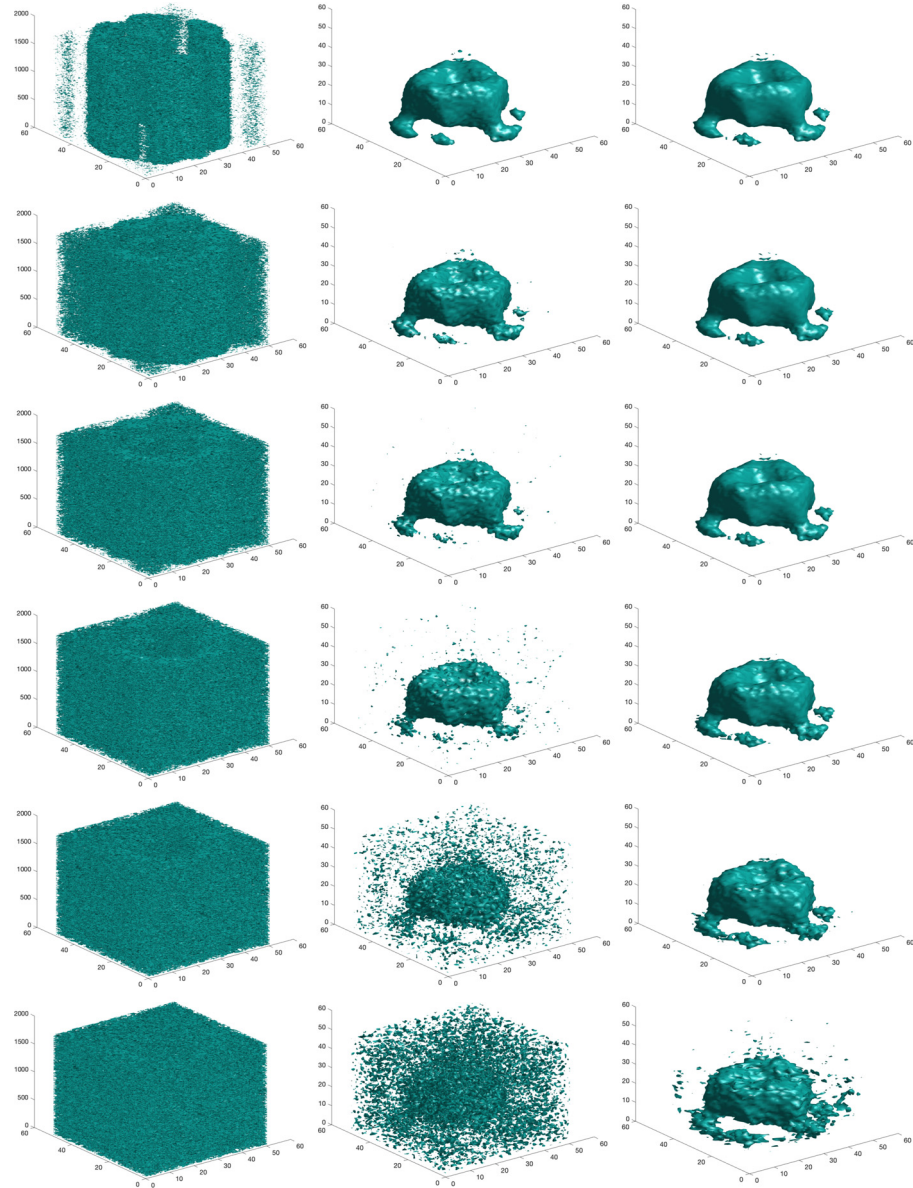


Fig. 3. The reconstruction results with different degradation at projection number 1800. From top to bottom: SNR = [4, 2, 1, 1/4, 1/16, 1/64]. The first column is the observed particle, the second column is the reconstructed result by the TV-based model [21], and the last column is ours.

regularizer, model (8) shows better noise suppression ability than (7) and has a better reconstruction effect. However, with the property of the total variation-based models, the artifact can be found in the results. Therefore, a more efficient reconstruction model in cryo-EM is urgently needed.

2.2. Weighted nuclear norm minimization

Since high-dimensional signals usually have low-rank characters, many low-rank-based models are proposed for various image processing tasks. Among them, the weighted nuclear norm minimization (WNNM) scheme has its superior. The WNNM model was first proposed by Zhang et al. [17] for gray image denoising. Given an observed gray image g , their model with a close-formed solution can be written as

$$\min_v \|g - v\|_2^2 + \|v\|_{*,w} \quad (9)$$

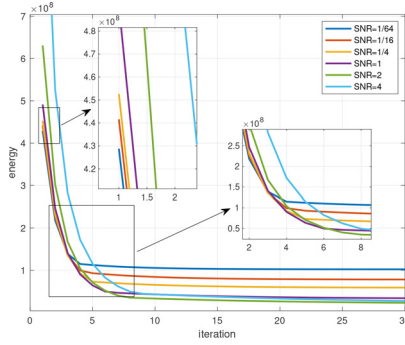
where v is the clean image, w is the weight. For each image patch v^j , the weight w_t is defined as

$$w_t = c\sqrt{n}/(\sigma_t(v^j) + \epsilon), \quad (10)$$

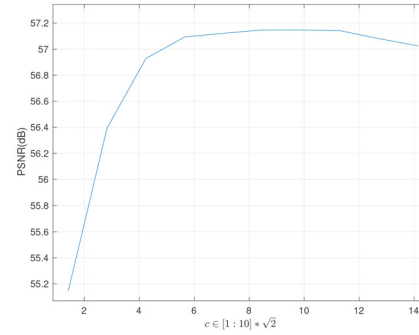
where $\sigma_t(v^j)$ is the t th singular value of v^j , c is a constant, n is the number of similar patches in image v , ϵ is a small parameter to avoid dividing by zero, and $\|\cdot\|_{*,w}$ is the weighted nuclear norm with $\|v\|_{*,w} = \sum_t w_t \sigma_t(v)$. Suppose the singular value decomposition of g is defined by $g = USV^*$, where U and V are permutation matrices, and S is the singular value matrix. If weights satisfy $\omega_1 \geq \omega_2 \geq \dots \geq \omega_m$, then

$$v = U\mathcal{P}_\omega(S)V^*, \quad (11)$$

where $\mathcal{P}_\omega(S)_{tt} = \max(S_{tt} - \omega_t, 0)$. For other orders of the weight ω_i , there are similar conclusions. A more comprehensive analysis of the WNNM model (9) can be found in Gu et al. [17]. Therefore, with the theoretical guarantee, there are various applications of the WNNM scheme. For example, Li et al. [19] proposed a phase



(a) The energy-decaying property.



(b) The weight ω analysis.

Fig. 4. (a) is the energy-decaying property of our method for particle 'emd_1022' with different noise levels. (b) is the PSNR values along with the weight ω .

retrieval model

$$\min_{\nu} \|g - |B\nu|\|_{\ell_{1-2}}^2 + \|\nu\|_{w,*}, \quad (12)$$

where B is an operator for phase retrieval, $\|\cdot\|_{\ell_{1-2}}$ represents the ℓ_{1-2} norm with $\|\nu\|_{\ell_{1-2}, \Omega_i} := \sum_{j \in \Omega_i} |\nu(j)| - \alpha (\sum_{j \in \Omega_i} |\nu(j)|^2)^{\frac{1}{2}}$, α was fixed as 0.5 in their paper. With the WNNM regularizer, they proposed a competitive model for phase retrieval with a closed-form solution. Zhang and Ng [34] proposed a model with a tensor nuclear norm minimization method. Moreover, they developed the convergence of a symmetric Gauss-Seidel based multiblock alternating direction method of multipliers to solve the proposed correction model. With the efficient algorithm, this completion model achieved promising results. However, when applying the WNNM regularizer to the three-dimensional cryo-EM task, two challenges emerge. On the one hand, the high-dimensional particle has many slices, which means the close-formed solution (11) is properly not guaranteed. On the other hand, as far as we know, a ready algorithm for a high-dimensional cryo-EM model is scarcely accessible. As a result, a three-dimensional WNNM-based reconstruction strategy is required.

2.3. Forward-backward splitting algorithm

Let \mathcal{H} be a Hilbert space, $f_1 : \mathcal{H} \rightarrow]-\infty, +\infty]$ and $f_2 : \mathcal{H} \rightarrow \mathbb{R}$ be two proper low semicontinuous convex functions such that f_2 is differentiable on \mathcal{H} with a $1/\beta$ -Lipschitz continuous gradient for some $\beta \in]0, +\infty[$. The symbol $]-\infty, +\infty]$ is the same as $(-\infty, +\infty]$ and $]-\infty, +\infty[$ is the same as $(-\infty, +\infty)$, which are the definition in the extended real-valued number system. The forward-backward splitting (FBS) algorithm [31] aims to find the solution of

$$\min_{x \in \mathcal{H}} f_1(x) + f_2(x). \quad (13)$$

Before presenting the existence, uniqueness, and characterization of the solution of the model (13), we give some basic notations first. Denote $\Gamma_0(\mathcal{H})$ as the class of all low semicontinuous convex functions from $\mathcal{H} \rightarrow]-\infty, +\infty]$ that are not identically $+\infty$. Denote $\Lambda(\mathcal{H})$ as the class of proper convex functions defined on \mathcal{H} . Let $\gamma \in]0, +\infty[$ and $\varphi \in \Gamma_0(\mathcal{H})$, for every $x \in \mathcal{H}$, the infimum in the continuous convex function

$$\gamma_\varphi : \mathcal{H} \rightarrow \mathbb{R} : x \mapsto \inf_{y \in \mathcal{H}} \varphi(y) + \frac{1}{2\gamma} \|x - y\|^2 \quad (14)$$

is achieved at a unique point $\text{prox}_{\gamma\varphi}x$, which is characterized by $x - \text{prox}_{\gamma\varphi}x \in \gamma\partial\varphi(\text{prox}_{\gamma\varphi}x)$. $\quad (15)$

The proximity operator of φ is therefore defined by

$$\text{prox}_\varphi : \mathcal{H} \rightarrow \mathcal{H} : x \mapsto \arg \min_{y \in \mathcal{H}} \varphi(y) + \frac{1}{2} \|x - y\|^2. \quad (16)$$

Proposition 2.1. According to Combettes and Wajs [35], we have

(i) Model (13) possesses at least one solution if $f_1 + f_2$ is coercive, i.e.,

$$\lim_{\|x\| \rightarrow +\infty} f_1(x) + f_2(x) = +\infty. \quad (17)$$

(ii) Model (13) possesses at most one solution if $f_1 + f_2$ is strictly convex. This happens especially when one of f_1 and f_2 is strictly convex.

(iii) Denote $x \in \mathcal{H}$ and $\gamma \in]0, +\infty[$. The following statements are equivalent.

(a) x is the solution of model (13);

(b) $x = \text{prox}_{\gamma f_1}(x - \gamma \nabla f_2(x))$;

(c) for any $y \in \mathcal{H}$, then $\langle x - y, \nabla f_2(x) \rangle + f_1(x) \leq f_1(y)$.

The proof of Proposition 2.1 can be found in the supplementary material Appendix A. In the FBS algorithm, Proposition 2.1 (iii)(b) suggested solving (13) with a suitable γ and the fixed point iteration

$$x_n = \text{prox}_{\gamma f_1}(x_n - \gamma \nabla f_2(x_n)). \quad (18)$$

Specifically, the FBS consists of the forward (explicit) step and backward (implicit) step, i.e.,

$$\begin{aligned} \text{Forward Step: } x_{n+\frac{1}{2}} &= x_n - \gamma \nabla f_2(x_n), & \text{Backward Step: } x_{n+1} \\ &= \text{prox}_{\gamma f_1} x_{n+\frac{1}{2}}. \end{aligned} \quad (19)$$

As a matter of fact, the formation (13) is suitable for most image processing minimization problems. For example, Ding and Han [36] proposed a method based on the FBS algorithm for maximal monotone mappings. Chang et al. [37] proposed a proximal alternating linearized minimization based on the FBS algorithm with global convergence. In [38], the authors proposed an FBS algorithm for image segmentation. However, the effectiveness of the FBS algorithm in cryo-EM reconstruction is still debatable. In this paper, we try to optimize the FBS algorithm to solve the proposed model and give the convergence analysis.

3. Our scheme

In this section, we present the proposed scheme for single-particle reconstruction (SPR) in cryogenic electron microscopy (cryo-EM). Owing to the robustness of the weighted nuclear norm minimization (WNNM) regularizer, we extend model (9) to three-dimension. Meanwhile, considering that the forward-backward splitting (FBS) algorithm has a close-formed solution with the explicit and implicit steps, we introduce the FBS to the proposed method.

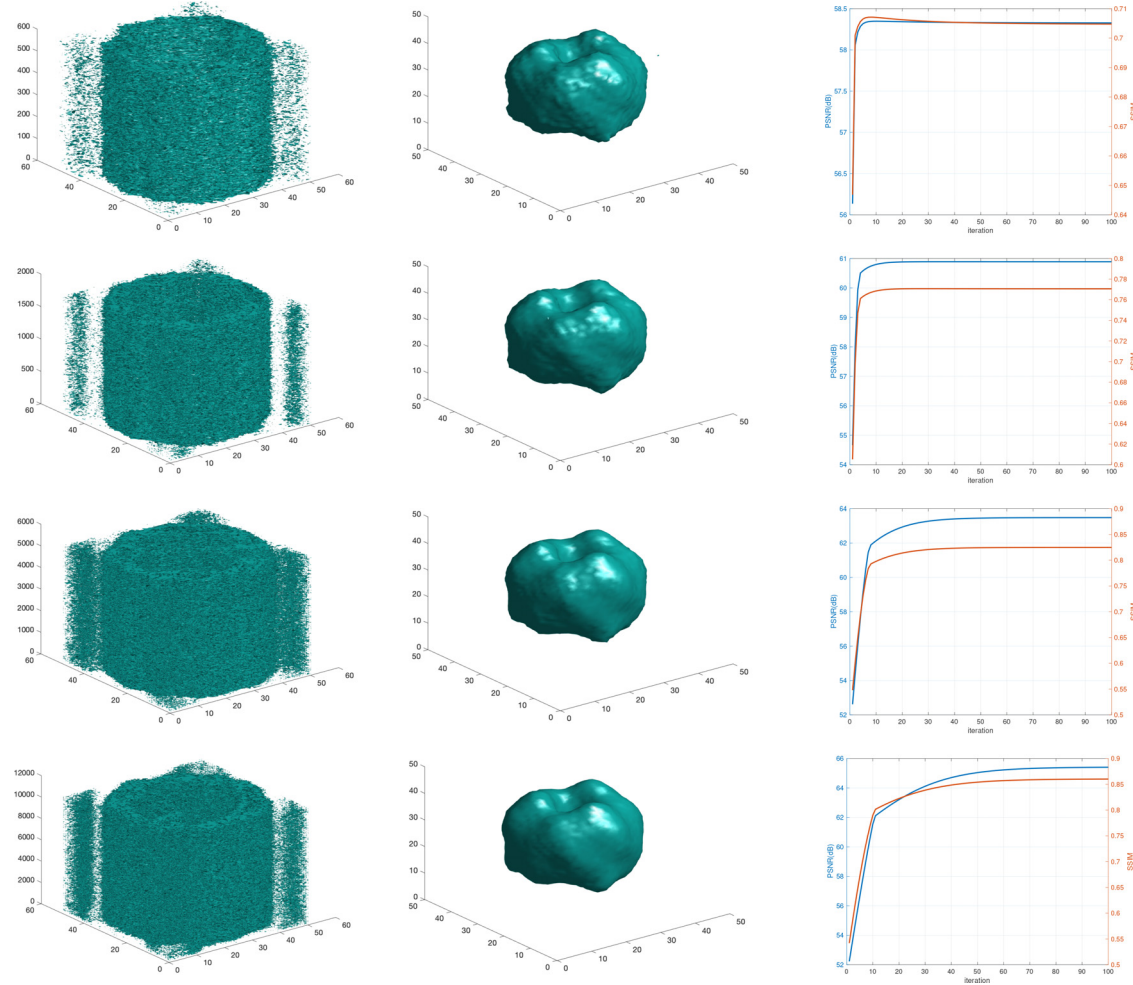


Fig. 5. The reconstruction results with different projection numbers under $\text{SNR} = 4$. From top to bottom: Projection number = [600, 1800, 5400, 10,800]. The first column is the observed particle, the second column is the reconstructed result by our method, and the last column is the PSNR (dB) and SSIM results corresponding to the reconstructed result. Obviously, as the number of projections increases, better reconstruction results can be obtained.

3.1. The proposed reconstruction model

We aim to find a single-particle v in a real Hilbert space \mathcal{H} from the observation g in a real Hilbert space \mathcal{G} . The CTF and other corrections mentioned in Section 2.1 are denoted as the linear operator A , so that the degradation formation is

$$g = Av + b, \quad (20)$$

where $b \in \mathcal{G}$ stands for an additive Gaussian noise. We intend to handle the three-dimensional SPR task and propose the reconstruction model as

$$\min_v \|v\|_{*,w} + \|Av - g\|^2, \quad (21)$$

where $\|\cdot\|_*$ is the nuclear norm and w is the weight. Specifically, $\|v\|_{*,w} = \sum_t \omega_t \sigma_t(v_i^j)$, $\sigma_t(v_i^j)$ is the t th singular value of v_i^j , and $\omega_t = \frac{c\sqrt{n}}{\sigma_t(v_i^j) + \epsilon}$ is the weight of patch v_i^j , $c > 0$ is a constant, n is the number of similar patches in the image v_i , $\epsilon > 0$ is a small number to avoid dividing by zero. It can be seen that the regularization parameter in the above formula is ω , and different singular values have different weights. Different from (9), there is a linear operator A that appeared in the data fidelity term and the minimization vary v is in three-dimension. As the proposed model (21) has two terms, let $f_1(v) = \|v\|_{*,w}$, $f_2(u) = \|Av - g\|^2$, and $\beta = 1/2\|A\|^2$, according to Section 2.3, the proposed model can be solved by the FBS algorithm. More specifically, we constrain

the model (21) under some conditions. Let (1) \mathcal{K} be a real Hilbert space; (2) $A : \mathcal{H} \rightarrow \mathcal{G}$ be a nonzero bounded linear operator; (3) $f_1(v) \in \Gamma_0(\mathcal{K})$; (4) \mathcal{G} be the set of solutions to model (21).

Proposition 3.1. *Model (21) is a special case of minimization problem (13) with $f_1(v) = \|v\|_{*,w}$, $f_2(u) = \|Av - g\|^2$, and $\beta = 1/2\|A\|^2$.*

Proof. Let $f_1(v) = \|v\|_{*,w}$ and $f_2(u) = \|Av - g\|^2$, then from the above conditions (1)–(4) we know that $f_1, f_2 \in \Gamma_0(\mathcal{H})$ and f_2 is differentiable on \mathcal{H} with $\nabla f_2(v) = 2A^*(Av - g)$. Then, for any v_1 and $v_2 \in \mathcal{H}$ we have

$$\begin{aligned} \|\nabla f_2(v_1) - \nabla f_2(v_2)\| &= \|2A^*(Av_1 - g) - 2A^*(Av_2 - g)\| \\ &= \|2A^*A(v_1 - v_2)\| \\ &\leq \|\sqrt{2}A\|^2 \|v_1 - v_2\|. \end{aligned} \quad (22)$$

Therefore, ∇f_2 is Lipschitz continuous with constant $2\|A\|^2$. \square

Remark 3.1. The WNNM model is generally nonconvex. However, when the weights w_i in (10) are in a non-ascending order, the problem (9) is still convex. Here we analyze the proposed model (21) with weights in a non-ascending order.

Given the FBS algorithm, the proposed model has the following properties.

Theorem 3.1.

- The minimization problem (21) possesses at least one solution if $f_1 + f_2$ is coercive.*

- (ii) The minimization problem (21) possesses at most one solution if one of the following conditions is satisfied:
- $f_1 + f_2$ is strictly convex;
 - A is injective.
- (iii) The minimization problem (21) possesses exactly one solution if A is bounded below, i.e.,
- $$(\exists \kappa \in]0, +\infty[) (\forall v \in \mathcal{H}) \|Av\| \geq \kappa \|v\|. \quad (23)$$

- (iv) Let $v \in \mathcal{H}$ and $\gamma \in]0, +\infty[$. The following statements are equivalent:
- v is the solution of model (21);
 - $v = \text{prox}_{\gamma f_1}(v - \gamma \nabla f_2(v))$;
 - for any $v_0 \in \mathcal{H}$, then $\langle v - v_0, 2A^*(Av - g) \rangle + f_1(v) \leq f_1(v_0)$.

The proof of **Theorem 3.1** can be found in the supplementary material Appendix B.

Next, we study the stability of the solution to model (21) with the observed data g .

Theorem 3.2. Suppose that A is bounded below, let g_1 and $g_2 \in \mathcal{G}$, v_1 and v_2 be the unique solutions to model (21) associated with g_1 and g_2 , respectively. Then we have

$$\|v_1 - v_2\| \leq \frac{\|g_1 - g_2\|}{\kappa}. \quad (24)$$

Proof. The uniqueness and the existence of model (21) are proposed in **Theorem 3.1**. Form **Theorem 3.1** (iv)(c), we know that

$$\begin{cases} \langle Av_1 - Av_2, g_2 - Av_2 \rangle + f_1(v_2) \leq f_1(v_1), \\ \langle Av_2 - Av_1, g_1 - Av_1 \rangle + f_1(v_1) \leq f_1(v_2), \end{cases} \quad (25)$$

then we have

$$\|A(v_1 - v_2)\|^2 \leq \langle A(v_1 - v_2), g_1 - g_2 \rangle. \quad (26)$$

By Cauchy-Schwarz inequality, we have

$$\|A(v_1 - v_2)\| \leq \|g_1 - g_2\|. \quad (27)$$

With $\|Av\| \geq \kappa \|v\|$, we then completed the proof. \square

Following [39], we study a more general iteration with improved convergence. First, the following condition is given.

Lemma 3.1. Let X be a nonempty set in Hilbert space \mathcal{H} , a function $\varphi \in \Gamma_0(\mathcal{H})$ satisfies this lemma on X if for all sequences $(y_n)_{n \in \mathbb{N}}$ and $(v_n)_{n \in \mathbb{N}} \in \mathcal{H}$, point $y \in X$ and $v \in \partial\varphi(y)$, there holds

$$[y_n \rightarrow y, v_n \rightarrow v, (\forall n \in \mathbb{N}) v_n \in \partial\varphi(y_n)] \Rightarrow y \text{ is a strong cluster point of } (y_n)_{n \in \mathbb{N}}. \quad (28)$$

Then the convergence result is given as follows.

Theorem 3.3. Suppose $G \neq \emptyset$. Let $(\gamma_n)_{n \in \mathbb{N}}$ be a sequence in $]0, +\infty[$ such that $0 < \inf_n \gamma_n \leq \sup_n \gamma_n < 2\beta$. Let $(\lambda_n)_{n \in \mathbb{N}}$ be a sequence in $]0, 1[$ such that $\inf_n \lambda_n > 0$. Let $(a_n)_{n \in \mathbb{N}}$ and $(b_n)_{n \in \mathbb{N}}$ be sequences in \mathcal{H} such that $\sum_n \|a_n\| < +\infty$ and $\sum_n \|b_n\| < +\infty$. Fix $x_0 \in \mathcal{H}$ and for every $n \in \mathbb{N}$, set

$$x_{n+1} = x_n + \lambda_n (\text{prox}_{\gamma_n f_1}(x_n - \gamma_n (\nabla f_2(x_n) + b_n)) + a_n - x_n). \quad (29)$$

Then the following holds.

- $(x_n)_{n \in \mathbb{N}}$ converges weakly to a point $x \in G$.
- $\sum_{n \in \mathbb{N}} \|\nabla f_2(x_n) - \nabla f_2(x)\|^2 < +\infty$.
- $\sum_{n \in \mathbb{N}} \|\text{prox}_{\gamma_n f_1}(x_n - \gamma_n \nabla f_2(x_n)) - x_n\|^2 < +\infty$.
- $(x_n)_{n \in \mathbb{N}}$ converges strongly to x if and only if $\lim_{n \rightarrow \infty} d_G(x_n) = 0$. In particular, strong convergence occurs in each of the following cases:
 - $\text{int } G \neq \emptyset$.

- f_1 satisfies Lemma 3.1 on G .
- f_2 satisfies Lemma 3.1 on G .

The proof of **Theorem 3.1** can be found in the supplementary material Appendix C.

3.2. The numerical scheme

For the proposed model (21), as mentioned in **Proposition 3.1** and the analysis in **Section 3.1**, let $f_1(v) = \|v\|_{*,w}$ and $f_2(v) = \|Av - g\|^2$, then we have

$$v^{k+1} = \text{prox}_{t f_1}(v^k - t \nabla f_2(v^k)), \quad (30)$$

where t is a positive parameter, $\text{prox}_{t f_1}(\cdot)$ is the proximal operator and defined as

$$\text{prox}_{t f_1}(u) := \arg \min_v \{f_1(v) + \frac{1}{2t} \|v - u\|^2\}. \quad (31)$$

Therefore, the final solution of model (21) is

$$v^{k+1} = \arg \min_v \|\nu\|_{*,w} + \frac{1}{2t} \|\nu - (v^k - t \nabla f_2(v^k))\|^2. \quad (32)$$

Therefore, the proposed SPR model can be solved by the FBS algorithm with theorem guaranteed. The proposed algorithm scheme is summarized in **Algorithm 1**.

Algorithm 1 The proposed scheme.

```

Input The observed  $g$ , operator  $A$ , iteration  $T$ , parameter  $t$ , and weight  $\omega$ ;
Initialization  $v^0 = g$ ;
for  $k = 1 : T$  do
  Forward step:  $u^{k+1} = v^k - tA^*(Av^k - g)$ ;
  Backward step:  $v^{k+1} = \text{prox}_{t f_1}(u^{k+1}) = \arg \min_v \|\nu\|_{*,w} + \frac{1}{2t} \|\nu - u^{k+1}\|^2$ ;
end for
return  $v^{k+1}$ .

```

4. Experiment

This section presents the numerical results and visual quality of the single-particle reconstruction (SPR) in cryo-EM. To demonstrate the effectiveness of the proposed three-dimensional weighted nuclear norm minimization (WNNM) model, we compare the proposed method with the total variation (TV)-based reconstruction approach (model (8)), the Tikhonov regularizer (Tik)-based algorithm (model (7)), and the adaptive Tikhonov regularizer (aTik)-based model (model (7) with adaptive parameter α). The test single particles¹ 'emd_1022', 'emd_1023', 'emd_1252' 'emd_1024', and 'emd_5505' are shown in **Fig. 2**.

4.1. The effectiveness of the proposed method

In this part, we test the performance of the proposed scheme with degradation under noise level cases measured by the signal-to-noise ratio (SNR), $\text{SNR} = [4, 2, 1, 1/4, 1/16, 1/64]$. As shown in **Fig. 3**, we provide the visual result of particle 'emd_1022' reconstructed by the proposed model and the TV-based method. According to the figure, we can see that as the SNR decreases, the proposed model has better robustness compared with the TV-based

¹ Single particles are collected from <https://www.ebi.ac.uk/embdb/>. Particle emd_1022 is with size $50 \times 50 \times 50$ and resolution 34.5 \AA , emd_1023 is with size $50 \times 50 \times 50$ and resolution 42.2 \AA , emd_1252 is with size $69 \times 69 \times 69$ and resolution 34.0 \AA , emd_1024 is with size $50 \times 50 \times 50$ and resolution 29.0 \AA , and emd_5505 is with size $54 \times 54 \times 54$ and resolution 20.0 \AA .

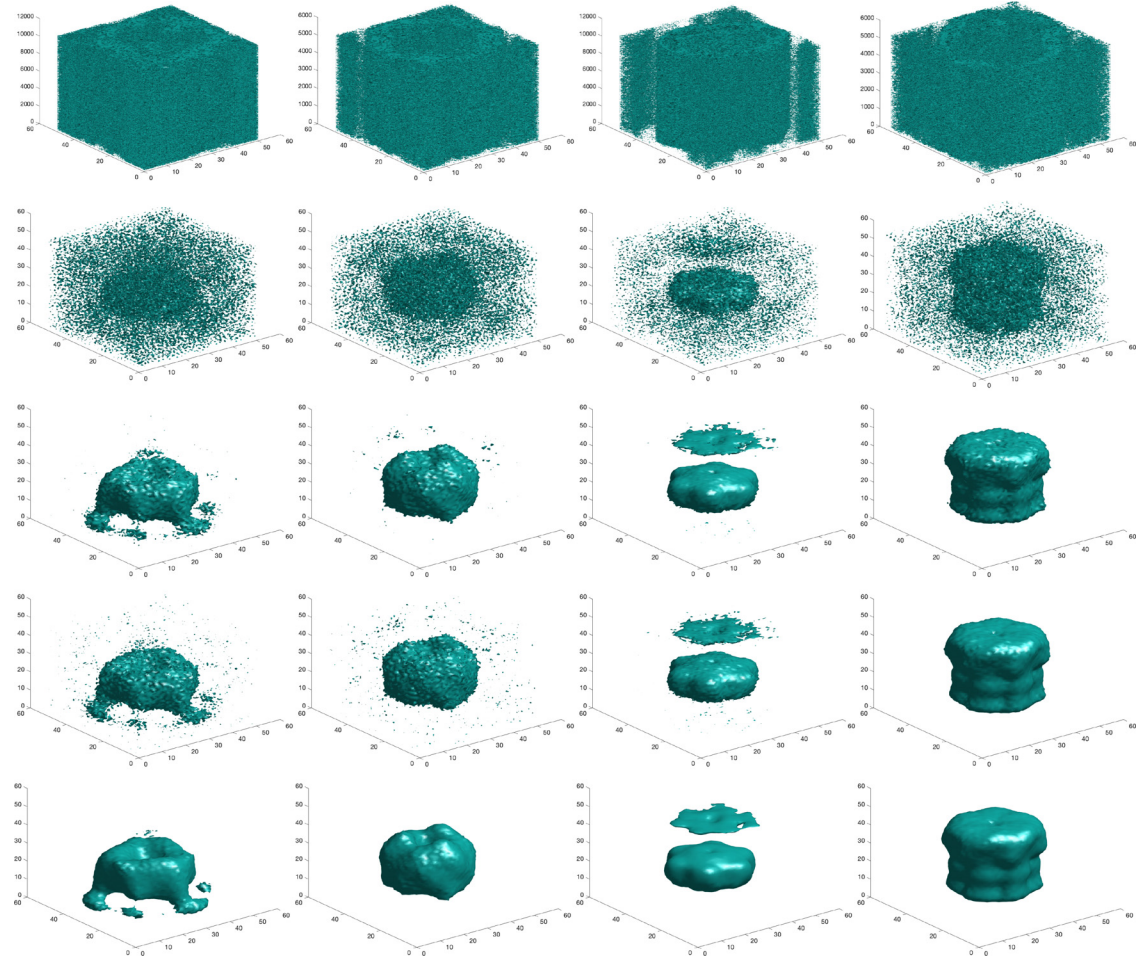


Fig. 6. Reconstruction results of different methods. From top to bottom: The degraded particle, reconstruction result by Tik, aTik, TV, and ours. The first column lists the single particle 'emd_1022' with the SNR = 1 and Projection number = 10,800. The second column lists the single particle 'emd_1023' with the SNR = 1 and Projection number = 5400. The third column lists the single particle 'emd_1024' with the SNR = 4 and Projection number = 10,800. The last column lists the single particle 'emd_5505' with the SNR = 2 and Projection number = 5400. Obviously, our model can reconstruct more accurate and smoother results.

method. Meanwhile, we show the energy-decaying property of our method in Fig. 4(a). Obviously, in all the test SNR values, the energy of our method is convergence stability, which demonstrates the proposed scheme is robust under different noise levels. As the proposed model (21) is with regularizer parameter ω , we conduct the analysis of the effect of the final results of ω in Fig. 4(b). The parameter c in QWNNM [9] was set to be $1.7 * \sqrt{2}$, here, we set $c \in [1 : 10] * \sqrt{2}$ with step size 0.1. Since the parameter ϵ is a small positive constant to avoid the denominator as zero. Hence, ϵ does not effectively affect the result, we set $\epsilon = \text{eps}$ for all our experiments. Meanwhile, c is a significant parameter in weight w_t . The choice of c is directly affecting weight w_t and the final result. Through trial and error, we set $c = 7.2 * \sqrt{2}$ for all our experiments.

4.2. Reconstruction with different projection numbers

Since the reconstruction of the three-dimensional particle is related to the number of projections, it is worth comparing the results with the different numbers of projections. Here we test the projection numbers at 600, 1800, 5400, and 10,800 to further illustrate the effectiveness of the proposed approach. The reconstruction results of 'emd_1023' with SNR = 4 are given in Fig. 5. The numerical curves of PSNR (left and blue line) and SSIM (right

and orange line) demonstrate that the reconstruction performance improves as the projection number increases.

4.3. Comparison with state-of-the-art algorithms

In this part, we compare the proposed model with the TV-based model, the Tik-based algorithm, and the aTik-based method on noise-corrupted particles with different projection numbers. In Table 1, we provide the average PSNR/SSIM comparison with these methods under different projection numbers and SNR. According to these results, we can clearly observe that our method achieves the best results in all cases. This fully demonstrates the effectiveness and excellence of our proposed method. Meanwhile, the reconstruction results are shown in Fig. 6. According to the figure, we can see that the proposed method can reconstruct better results compared with others. This experiment further verifies the effectiveness of the proposed method.

For a particle with a more complex structure ('emd_1252'), we present the reconstruction results in Fig. 7. The reconstruction task with heavy noise in the particle 'emd_1252' is more challenging since some structures will be misidentified as noise. However, using a low noise level algorithm leaves some noise in the reconstructed particles. In general, the proposed model has competitive performance in reconstructing the particle with complex struc-

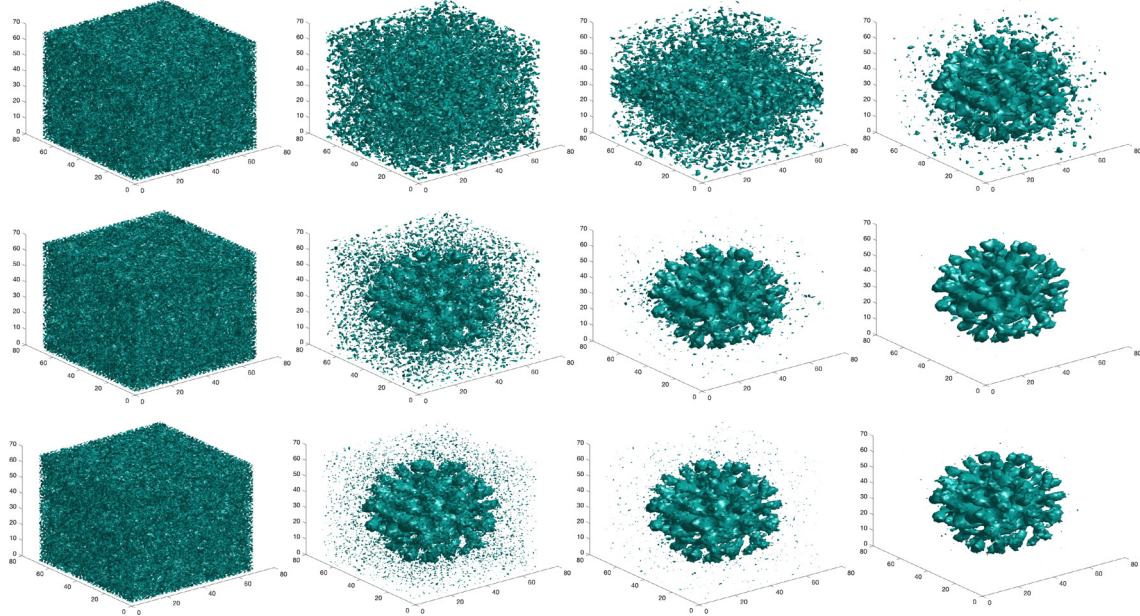


Fig. 7. Reconstruction results of particle 'emd_1252'. From left to right: The reconstruction results by Tik, aTik, TV, and ours. The first row is with the SNR = 1/16 and Projection number = 1800. The second row is with the SNR = 0.25 and Projection number = 5400. The third row is with the SNR = 1 and Projection number = 10,800. With the increasing of projection numbers and the SNR levels, the reconstruction results get better.

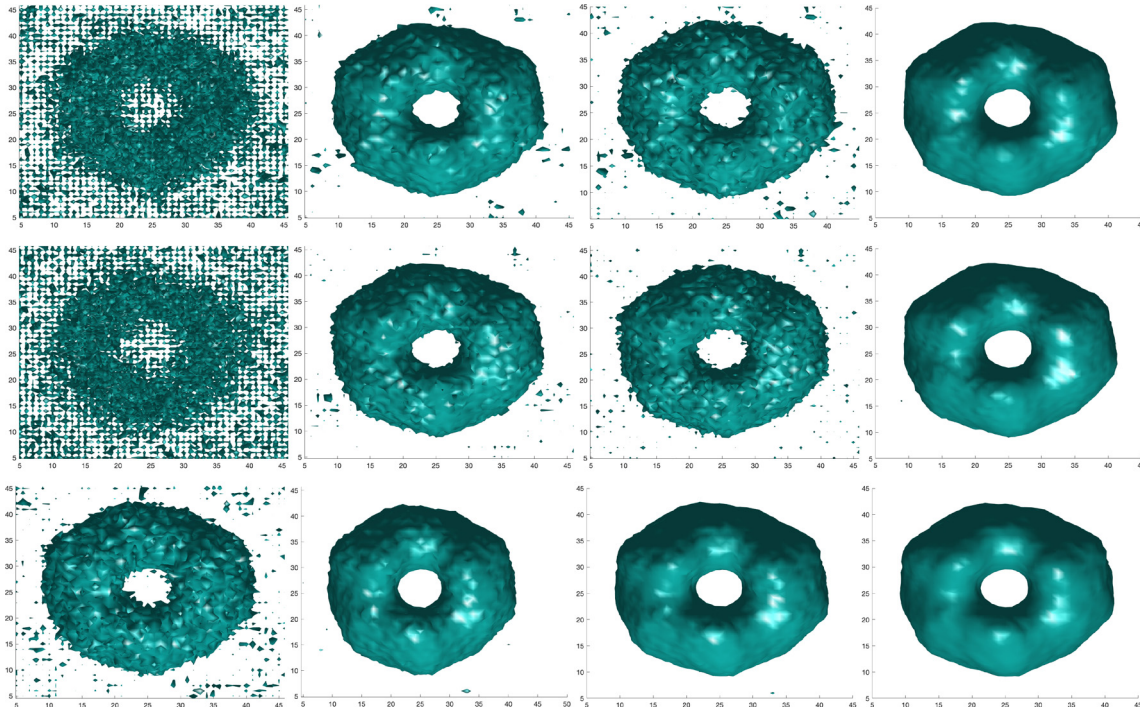


Fig. 8. Reconstruction results of particle 'emd_1023' (from v_3 -axis angle). From left to right: The reconstruction results by Tik, aTik, TV, and ours. The first row is with the SNR = 1 and Projection number = 5400. The second row is with the SNR = 1 and Projection number = 10,800. The third row is with the SNR = 4 and Projection number = 600.

tures. Although with the projection number set to 10,800, the results still show some noise around the particle, our scheme is superior to other compared state-of-the-art methods. In the future, we aim to explore a more fixable model to handle particle reconstruction with complex structures.

Different from the other particle, the topology of particle 'emd_1023' is of genus-1. To better present the particle 'emd_1023',

we rotate the particles. As can be seen from Fig. 8, the particle in the top view is of genus-1 attributes. The difficulty in reconstructing the genus-1 is that the heavy noise will fulfill the hole in the particle so that the noise can not be removed easier. With the SNR = 1, the surface inside the particle is not well reconstructed, i.e., the holes are not perfect as the original particle's. The reconstruction results are much better in the condi-

Table 1

Average PSNR/SSIM comparison with other methods under different projection numbers [600, 1800, 5400, 10,800] and SNR [4, 2, 1, 1/4, 1/16, 1/64]. The best results are **highlighted**.

method	Projection number = 600					
	SNR = 4	SNR = 2	SNR = 1	SNR = 1/4	SNR = 1/16	SNR = 1/64
Tik	42.15/0.1130	37.74/0.0495	34.04/0.0223	27.54/0.0048	21.42/0.0011	15.41/0.0002
aTik	63.26/0.6711	59.26/0.4525	57.39/ 0.7678	55.63/0.3671	53.70/0.4070	50.86/ 0.2701
TV	66.73/0.7338	65.09/0.4890	62.95/0.5040	59.64/0.3839	54.23/0.4013	51.04/0.2594
Ours	68.09/0.7554	66.33/0.7165	64.55/0.6737	60.92/0.5707	56.75/0.4184	53.43/0.2601
Projection number = 1800						
Tik	46.65/0.2142	41.03/0.0915	36.69/0.0389	29.70/0.0077	23.46/0.0016	17.40/0.0004
aTik	63.71/0.6691	62.81/0.5765	62.02/0.3579	61.80/0.5411	57.60/0.4511	54.80/0.2951
TV	68.41/0.7773	67.93/0.6278	65.14/0.6120	63.71/0.5026	58.29/0.4363	54.29/0.3274
Ours	70.62/0.8087	68.89/0.7750	67.18/0.7390	63.89/0.6584	60.32/0.5550	56.07/0.3916
Projection number = 5400						
Tik	52.13/0.3611	45.38/0.1789	39.74/0.0700	31.57/0.0113	25.01/0.0022	18.86/0.0004
aTik	64.11/0.6952	66.67/0.6791	63.04/0.6310	59.16/0.5514	57.97/0.4980	55.60/0.3300
TV	71.69/0.8305	69.51/0.6740	66.21/0.6577	65.59/0.5845	60.56/0.4886	56.32/0.3873
Ours	73.17/0.8547	71.38/0.8245	69.64/0.7917	66.27/0.7163	62.44/0.6155	57.74/0.4783
Projection number = 10,800						
Tik	52.57/0.3683	46.63/0.2052	40.73/0.0806	31.32/0.0098	23.85/0.0015	17.28/0.0003
aTik	68.91/0.7721	67.03/0.7537	63.98/0.7465	64.28/0.7229	59.96/0.6123	53.89/0.3328
TV	72.98/0.8468	71.17/0.8213	68.83/0.7788	65.42/0.6905	64.92/0.5897	58.53/0.3592
Ours	73.79/0.8815	71.86/0.8497	69.05/0.7939	67.31/0.7234	65.98/0.6514	59.89/0.3878

tion of a relatively high-level $\text{SNR} = 4$. The results of genus-0 and genus-1 demonstrate the proposed scheme's effectiveness and robustness.

5. Conclusion

This paper proposed a novel three-dimensional reconstruction scheme for single-particle reconstruction (SPR) in Cryo-EM. This scheme consists of a new weighted nuclear norm minimization (WNNM) with three-dimensional energy and an efficient energy-decaying forward-backward splitting (FBS) algorithm. The proposed three-dimensional WNNM model and the FBS algorithm significantly improved the performance of the reconstruction task with different noise levels and projection numbers in cryo-EM. Furthermore, we have analyzed and given the convergence guarantee of the proposed model. Experiments demonstrate the robustness and the energy-decaying propriety of our method. Compared with the existing approaches, the proposed method has better performance in terms of reconstruction quality. Since the SPR in Cryo-EM is still in its early stage, in this paper, we only consider reconstruction with fixed and known orientations and positions. In the future, we will consider studying the construction with different viewing directions to better synthesize the accurate imaging. Besides, we only analyze the convergence and consistency with the non-ascending order of the weight in the 3DWNNM model. We will study the non-convex condition in the next work to perfect the theoretical analysis. Furthermore, the weighted nuclear norm minimization and total variation are combined in several image processing works. We believe this combination in three-dimensional also worked. In future work, we will further improve our research by combining these two regularizers to handle three-dimensional tasks.

Declaration of Competing Interest

The authors declare that they have no known competing financial interests or personal relationships that could have appeared to influence the work reported in this paper.

Data availability

No data was used for the research described in the article.

Acknowledgment

The research was in part by the [National Key R&D Program of China](#) under Grant [2021YFE0203700](#), Grant [NSFC/RGC N_CUHK 415/19](#), Grant [ITF MHP/038/20](#), Grant [RGC 14300219, 14302920, 14301121](#), and CUHK Direct Grant for Research under Grant [4053405, 4053460](#), the [Natural Science Foundation of China](#) under Grant [61971234, 12126340, 12126304, 11501301, 12090022](#) the “QingLan” Project for Colleges and Universities of Jiangsu Province, the [Natural Science Foundation of Shanghai](#) under Grand [23ZR1422200](#), the Shanghai Sailing Program under Grant [23YF1412800](#).

Supplementary material

Supplementary material associated with this article can be found, in the online version, at [10.1016/j.patcog.2023.109736](#).

References

- [1] E. Katsevich, A. Katsevich, A. Singer, Covariance matrix estimation for the cryo-EM heterogeneity problem, *SIAM J. Imaging Sci.* 8 (1) (2015) 126–185.
- [2] B. Li, C. Shen, Y. Chi, M. Yang, Y. Lou, L. Zhou, X. Jia, Multispectral cone-beam computed tomography reconstruction with a spatial spectral nonlocal means algorithm, *SIAM J. Imaging Sci.* 11 (2) (2018) 1205–1229.
- [3] C. Wang, M. Tao, J.G. Nagy, Y. Lou, Limited-angle CT reconstruction via the L_1/L_2 minimization, *SIAM J. Imaging Sci.* 14 (2) (2021) 749–777.
- [4] Y. Chen, T.-Z. Huang, W. He, N. Yokoya, X.-L. Zhao, Hyperspectral image compressive sensing reconstruction using subspace-based nonlocal tensor ring decomposition, *IEEE Trans. Image Process.* 29 (2020) 6813–6828.
- [5] Q. Dai, F. Fang, J. Li, G. Zhang, A. Zhou, Edge-guided composition network for image stitching, *Pattern Recognit.* 118 (2021) 108019.
- [6] M.K. Ng, X. Zhang, X.-L. Zhao, Patched-tube unitary transform for robust tensor completion, *Pattern Recognit.* 100 (2020) 107181.
- [7] Y. Xu, S. Chen, J. Li, L. Luo, J. Yang, Learnable low-rank latent dictionary for subspace clustering, *Pattern Recognit.* 120 (2021) 108142.
- [8] G. Song, W. Ding, M.K. Ng, Low rank pure quaternion approximation for pure quaternion matrices, *SIAM J. Matrix Anal. Appl.* 42 (1) (2021) 58–82.
- [9] C. Huang, Z. Li, Y. Liu, T. Wu, T. Zeng, Quaternion-based weighted nuclear norm minimization for color image restoration, *Pattern Recognit.* 128 (2022) 108665.
- [10] T.-X. Jiang, M.K. Ng, X.-L. Zhao, T.-Z. Huang, Framelet representation of tensor nuclear norm for third-order tensor completion, *IEEE Trans. Image Process.* 29 (2020) 7233–7244.
- [11] J. Pan, M.K. Ng, Orthogonal nonnegative matrix factorization by sparsity and nuclear norm optimization, *SIAM J. Matrix Anal. Appl.* 39 (2) (2018) 856–875.
- [12] G. Gao, J. Yang, X.-Y. Jing, F. Shen, W. Yang, D. Yue, Learning robust and discriminative low-rank representations for face recognition with occlusion, *Pattern Recognit.* 66 (2017) 129–143.

- [13] J. Zeng, G. Cheung, M.K. Ng, J. Pang, C. Yang, 3D point cloud denoising using graph Laplacian regularization of a low dimensional manifold model, *IEEE Trans. Image Process.* 29 (2019) 3474–3489.
- [14] L. Luo, J. Yang, Y. Zhang, Y. Xu, H. Huang, Nesting-structured nuclear norm minimization for spatially correlated matrix variate, *Pattern Recognit.* 91 (2019) 147–161.
- [15] J.-H. Yang, X.-L. Zhao, T.-H. Ma, Y. Chen, T.-Z. Huang, M. Ding, Remote sensing images destriping using unidirectional hybrid total variation and nonconvex low-rank regularization, *J. Comput. Appl. Math.* 363 (2020) 124–144.
- [16] T.-Y. Ji, T.-Z. Huang, X.-L. Zhao, T.-H. Ma, L.-J. Deng, A non-convex tensor rank approximation for tensor completion, *Appl. Math. Model.* 48 (2017) 410–422.
- [17] S. Gu, L. Zhang, W. Zuo, X. Feng, Weighted nuclear norm minimization with application to image denoising, in: *Proceedings of the IEEE Conference on Computer Vision and Pattern Recognition*, 2014, pp. 2862–2869.
- [18] X.-G. Lv, F. Li, An iterative decoupled method with weighted nuclear norm minimization for image restoration, *Int. J. Comput. Math.* 97 (3) (2020) 602–623.
- [19] Z. Li, M. Yan, T. Zeng, G. Zhang, Phase retrieval from incomplete data via weighted nuclear norm minimization, *Pattern Recognit.* (2022) 108537.
- [20] T.-X. Jiang, T.-Z. Huang, X.-L. Zhao, L.-J. Deng, Multi-dimensional imaging data recovery via minimizing the partial sum of tubal nuclear norm, *J. Comput. Appl. Math.* 372 (2020) 112680.
- [21] H. Pan, Y.-W. Wen, T. Zeng, Constrained total variation based three-dimension single particle reconstruction in cryogenic electron microscopy, *J. Sci. Comput.* 85 (2) (2020) 37:1–20.
- [22] H. Pan, Y.-W. Wen, T. Zeng, A fast iterative shrinkage thresholding algorithm for single particle reconstruction of cryo-EM, in: *2018 IEEE 3rd International Conference on Image, Vision and Computing (ICIVC)*, IEEE, 2018, pp. 342–346.
- [23] W. Chen, M. Liu, H. Du, M. Radojević, Y. Wang, E. Meijering, Deep-learning-based automated neuron reconstruction from 3D microscopy images using synthetic training images, *IEEE Trans. Med. Imaging* 41 (5) (2021) 1031–1042.
- [24] B. Yang, M. Liu, Y. Wang, K. Zhang, E. Meijering, Structure-guided segmentation for 3D neuron reconstruction, *IEEE Trans. Med. Imaging* 41 (4) (2021) 903–914.
- [25] J.D. Yun, Y. Kim, Two-stage adaptive random Fourier sampling method for image reconstruction, *Pattern Recognit.* 117 (2021) 107990.
- [26] L. Wang, A. Singer, Z. Wen, Orientation determination of cryo-EM images using least unsquared deviations, *SIAM J. Imaging Sci.* 6 (4) (2013) 2450–2483.
- [27] L. Wang, Y. Shkolnisky, A. Singer, A fourier-based approach for iterative 3D reconstruction from cryo-EM images, *arXiv preprint arXiv:1307.5824*(2013b) 1–17.
- [28] L. Ma, L. Xu, T. Zeng, Low rank prior and total variation regularization for image deblurring, *J. Sci. Comput.* 70 (3) (2017) 1336–1357.
- [29] C. Chen, R.H. Chan, S. Ma, J. Yang, Inertial proximal ADMM for linearly constrained separable convex optimization, *SIAM J. Imaging Sci.* 8 (4) (2015) 2239–2267.
- [30] C. Chen, B. He, Y. Ye, X. Yuan, The direct extension of ADMM for multi-block convex minimization problems is not necessarily convergent, *Math. Program.* 155 (1) (2016) 57–79.
- [31] J.J. Moreau, Fonctions convexes duales et points proximaux dans un espace hilbertien, *C. R. Hebd. Séances Acad. Sci.* 255 (1962) 2897–2899.
- [32] T. Bendory, A. Bartesaghi, A. Singer, Single-particle cryo-electron microscopy: mathematical theory, computational challenges, and opportunities, *IEEE Signal Process. Mag.* 37 (2) (2020) 58–76.
- [33] Y. Li, X. Song, S. Kwak, J. Kim, Weighted 3D volume reconstruction from series of slice data using a modified Allen–Cahn equation, *Pattern Recognit.* 132 (2022) 108914.
- [34] X. Zhang, M.K. Ng, A corrected tensor nuclear norm minimization method for noisy low-rank tensor completion, *SIAM J. Imaging Sci.* 12 (2) (2019) 1231–1273.
- [35] P.L. Combettes, V.R. Wajs, Signal recovery by proximal forward-backward splitting, *Multiscale Model. Simul.* 4 (4) (2005) 1168–1200.
- [36] X. Ding, D. Han, A modification of the forward-backward splitting method for maximal monotone mappings, *Numer. Algebra, Control Optim.* 3 (2) (2013) 295–307.
- [37] H. Chang, S. Marchesini, Y. Lou, T. Zeng, Variational phase retrieval with globally convergent preconditioned proximal algorithm, *SIAM J. Imaging Sci.* 11 (1) (2018) 56–93.
- [38] S. Yan, J. Liu, H. Huang, X.-C. Tai, A dual EM algorithm for TV regularized gaussian mixture model in image segmentation, *Inverse Probl. Imaging* 13 (3) (2019) 653.
- [39] P.L. Combettes, Solving monotone inclusions via compositions of nonexpansive averaged operators, *Optimization* 53 (5–6) (2004) 475–504.

Chaoyan Huang is currently a Ph.D. student in the Department of Mathematics, The Chinese University of Hong Kong. She received the M.S. degree in the School of Science, Nanjing University of Posts and Telecommunications, Nanjing, China, in 2022. Her research interests include image processing and machine learning.

Tingting Wu is currently an Associate Professor in the School of Science, Nanjing University of Posts and Telecommunications, Nanjing, China. She received the B.S. and Ph.D. degrees in mathematics from Hunan University, Changsha, China, in 2006 and 2011, respectively. In 2015–2018, she was a Post-Doctoral Researcher with the School of Mathematical Sciences, Nanjing Normal University, Nanjing, China. In 2016–2017, she was a Research Fellow in Nanyang Technological University, Singapore. Her research interests include variational methods for image processing and computer vision, optimization methods and their applications in sparse recovery and regularized inverse problems.

Juncheng Li is currently a Assistant Professor in School of Communication & Information Engineering, Shanghai University. He received the Ph.D. from the School of Computer Science and Technology, East China Normal University (ECNU), China, in 2021. His research interests include image restoration, computer vision, deep learning, and medical image processing. He has published more than 30 scientific papers in IEEE TIP, IEEE TNNL, PR, ICCV, ECCV, etc.

Bin Dong is currently a Professor in Beijing International Center for Mathematical Research, Peking University. He received the B.S. from Peking University in 2003, M.Sc. from the National University of Singapore in 2005, and Ph.D. from the University of California Los Angeles (UCLA) in 2009. Then he spent 2 years in the University of California San Diego (UCSD) as a visiting assistant professor. He was a tenure-track assistant professor at the University of Arizona since 2011 and joined Peking University as an associate professor in 2014. His research interest is in mathematical modeling and computations in imaging and data analysis.

Tieyong Zeng is currently a Professor in the Department of Mathematics, The Chinese University of Hong Kong. Together with colleagues, he has founded the Center for Mathematical Artificial Intelligence (CMAI) since 2020 and served as the director of CMAI. He received the B.S. degree from Peking University, Beijing, China, the M.S. degree from Ecole Polytechnique, Palaiseau, France, and the Ph.D. degree from the University of Paris XIII, Paris, France, in 2000, 2004, and 2007, respectively. His research interests include image processing, optimization, artificial intelligence, scientific computing, computer vision, machine learning, and inverse problems.